Principles and Evaluation of Autostereoscopic Photogrammetric Measurement

Jie Shan, Chiung-Shiuan Fu, Bin Li, James Bethel, Jeffrey Kretsch, and Edward Mikhail

Abstract

Stereoscopic perception is a basic requirement for photogrammetric 3D measurement and accurate geospatial data collection. Ordinary stereoscopic techniques require operators wearing glasses or using eyepieces for interpretation and measurement. However, the recent emerging autostereoscopic technology makes it possible to eliminate this requirement. This paper studies the principles and implementation of autostereoscopic photogrammetric measurement and evaluates its performance. We first describe the principles and properties of the parallax barrier-based autostereoscopic display used in this study. As an important metric property, we quantitatively present the autostereoscopic geometry, including viewing zones and the boundary of a viewer's movement for autostereoscopic measurement. A toolkit AUTO3D is developed that has common photogrammetric functions. The implementation principles are described by addressing the differences compared to the ordinary stereoscopic technology. To evaluate the performance of the autostereoscopic measurement, images at a resolution of 25 μm and 50 μm are measured by a group of seven (7) operators, who are asked to digitize 18 well-defined roof points and 18 ground points. These results are evaluated by comparing the same measurements obtained from a popular stereoscopic photogrammetric workstation. It is shown that the precision of autostereoscopic measurement is about 16 percent to 25 percent lower than the conventional stereo workstation.

Introduction

Accurate and realistic 3D data collection requires stereoscopic perception and measurement. Throughout the history of photogrammetry for over 150 years, this requirement has been met by merely using eyepieces or glasses attached to the equipment or operators. However, recent development in autostereoscopic technology provides alternatives to this convention. In contrast to the traditional stereo technology, autostereo is goggle-free or aid-free (Okoshi 1976; Eichenlaub and Martens, 1990; Pastoor and Wöpking, 1997). Its potential utilization in photogrammetric practice has been brought to the attention of photogrammetrists and photogrammetry vendors (Petrie, 2001).

However, so far, the primary application fields of this technology are collective visualization and the entertainment industry with only limited application in geospatial data display. Jones and McLaurin (1993) take advantage of the capability of video and computer technology to rapidly display alternating pairs of remote sensing images. Usery (2003) discusses the critical issues such as color, resolution, and refresh rate for autostereoscopic display of geospatial data. Despite these visualization-oriented studies, properties and performance of autostereoscopic measurement are unknown to the photogrammetric community. In this paper, we focus on the metric properties of the autostereoscopic display and evaluate its performance for photogrammetric measurement. The paper starts with a brief introduction to the principles of the autostereoscopic technology. As an important metric property, we quantitatively show the autostereoscopic geometry, including viewing zones and the boundary of operator's movement for autostereoscopic perception. To carry out autostereoscopic measurement and evaluate its performance, a photogrammetric toolkit, AUTO3D, is developed based on a DTI (Dimension Technologies, Inc., 2004) autostereoscopic monitor. Principles and design considerations in the AUTO3D development are discussed. Finally, we compare the autostereoscopic measurement results with the ones obtained from a conventional stereo photogrammetric workstation. Seven (7) operators are involved in the tests by measuring a number of carefully selected feature points. The results and discussion of the experiments are presented in this paper.

Autostereoscopic Principle

The term "autostereoscope" is used to refer that a viewer can perceive 3D without viewing aids, such as goggles or eyepieces. The most popular autostereoscopic technology is based on the parallax barrier principle (Kaplan, 1952; Okoshi, 1976; Sexton, 1992). As shown in Figure 1, a specially designed image, called parallax stereogram, is placed behind a barrier made of opaque material with fine transparent vertical slits. The parallax stereogram is composed of (vertically) interleaved stripes from the left and right images of a stereo pair. Each transparent slit acts as a window to the corresponding image stripes. The image and the barrier are arranged in such a way that the left eye and right eye of the viewer at certain location will respectively see the left image and right image, so that the stereoscopic effect can be obtained.

In practice, this principle can be implemented differently for different autostereoscopic monitors. The key is to generate the parallax barrier. In the popular lenticular autostereoscopic technology, a plate or sheet with an array of small cylindrical lenses (lenticular plate) is used as the

Jie Shan, Chiung-Shiuan Fu, Bin Li, James Bethel, and Edward Mikhail are with Geomatics Engineering, School of Civil Engineering, Purdue University, 550 Stadium Mall Drive, West Lafayette, IN 47907-2051 (jshan@ecn.purdue.edu).

Jeffrey Kretsch is with the National Geospatial-Intelligence Agency.

Photogrammetric Engineering & Remote Sensing
Vol. 72, No. 4, April 2006, pp. 365–372.

0099-1112/06/7204–0365/$3.00/0

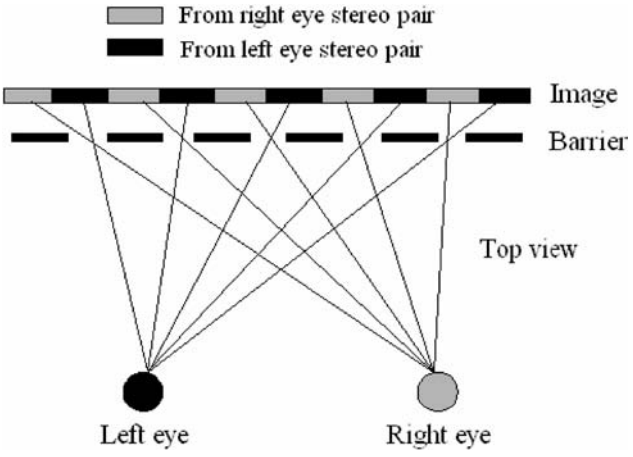

Figure 1. Principle of parallax barrier autostereoscope **(From http://astronomy.swin.edu.au/~pbourke/stereographics/lenticular/)**.

parallax barrier (Okoshi, 1976; Pastoor and Wöpking, 1997). The lenticular plate is designed and placed in front of the parallax stereogram in such a way that a viewer's left eye and right eye can only respectively see the left image and right image to achieve the stereo effect. As for the autostereoscopic monitor used in this study, it is implemented by a different technique as will be addressed below.

DTI Autostereoscopic Monitor

The autostereoscopic monitor 2018XL made by DTI is used in this study. The parallax barrier is formed by the so-called parallax illumination technique (Eichenlaub, 1993). As shown in Figure 2, an illumination plate is placed behind and spaced apart from the Liquid Crystal Display (LCD) display plane. It produces a large number of thin, bright vertical illuminating lines with dark space in between. There

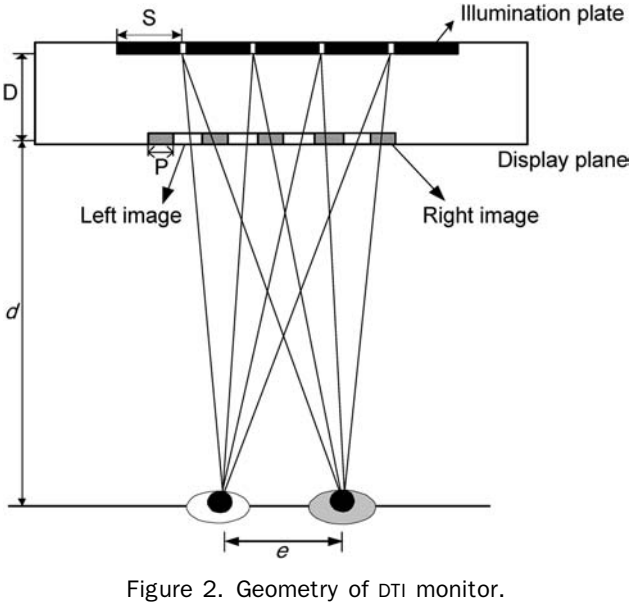

Figure 2. Geometry of DTI monitor.

Table 1. Specifications of the DTI 2018XL Monitor

Display Size	46 cm (18″)
Display Type	TFT LCD
Max. Display Resolution	1280 × 1024
Computer Resolution Supported	640 × 480 @ 60 Hz*; 800 × 600 @ 60 Hz*; 1024 × 768 @ 60 Hz*; 1284 × 1024 @ 60 Hz; 720 × 400 @ 70 Hz* (PC text mode) *Resolutions other than 1280 × 1024 are scaled to full-screen.
User Control	2D/3D; 3D Mode; Stereo Reverse on/off
Display Area	35.9 cm (W) × 28.7 cm (H)
Pixel size	0.2805 mm (H) × 0.2805 mm (V)
Display Colors	16.7 million (24-bit color, 8 bits/color)
Viewing Distance	71.1 cm +/−10.2 cm

is one bright line for every two columns of pixels. The lines are spaced such that a viewer sitting at the average viewing distance from the display sees all of the light lines through the odd columns of pixels with the left eye and the same set of light lines through the even columns of pixels with the right eye. In this way, the illumination plate actually plays the role of the required parallax barrier. Shown in Figure 2 is the geometry of the DTI monitor, where S is the distance between two light lines or the pitch of the parallax barrier; D is the distance between the LCD display plane and the illumination plate; P is the pixel width of the monitor; e is the eye base and d the viewing distance perpendicular to the monitor plane. As a result of this design, the monitor is 2D and 3D switchable. Namely, when the light lines are turned off, the monitor can be used as a common 2D monitor, which we regard as an important feature in order to display ordinary computer programs that are not specifically designed for autostereoscopic applications. A summary of the main specifications of the DTI monitor used in this study is listed in Table 1 (Dimension Technologies, Inc., 2004).

Viewing Geometry

The principle of the autostereoscopic display requires that a viewer stays in a certain range relative to the monitor to acquire stereo effect. This section studies the viewing geometry through theoretic reduction. As shown in Figure 2, the geometry of similar triangles yields the following relationships (Eichenlaub, 1993):

$$\frac{\mathrm{P}}{\mathrm{D}} = \frac{e}{d + \mathrm{D}} \tag{1}$$

$$\frac{2\mathrm{P}}{\mathrm{S}} = \frac{d}{d + \mathrm{D}} \quad \text{or} \quad \mathrm{S} = \frac{2\mathrm{P}(d + \mathrm{D})}{d}. \tag{2}$$

Combining Equations 1 and 2 produces

$$\frac{e}{d} = \frac{\mathrm{S}}{2\mathrm{D}} \tag{3}$$

where S is the distance between two light lines or the pitch of the parallax barrier; D is the distance between the LCD display plane and the illumination plate; d the viewing distance perpendicular to the monitor plane; and e is the eye base.

Equation 3 reveals the basic relationship in the (parallax barrier based) autostereoscope. It shows that the ratio of the eye base and the viewing distance needs to be equal to a constant related to the monitor manufacture to obtain the best stereo effect. This constant essentially is half of the ratio between the pitch and the illumination plate's distance to the monitor. To achieve the best stereo effect, one needs to adjust his or her distance to the monitor. In manufacture, the monitor parameters (D and S) are so

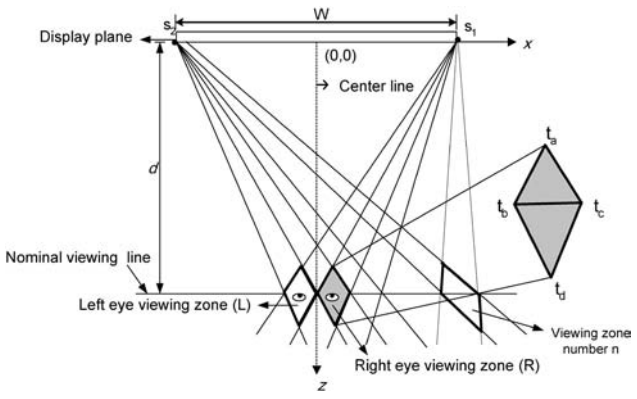

Figure 3. Geometry of the viewing zones.

designed that the best stereo effect can be obtained for an ordinary viewer (eye base of 6.5 cm) sitting at an average arm distance (75 cm) (Eichenlaub, 1993).

Another autostereoscopic property is the existence of viewing zones, within which a viewer can receive stereo effect. Figure 3 shows the geometry of viewing zones. Human heads can move horizontally in parallel to the monitor plane. Every movement at an interval of the eye base will ensure the right stereo effect. This property implies that multiple viewers can perceive stereo at the same time, if they are positioned at the right places (Son *et al.*, 2003). For a monitor with width W and a viewer with eye base e, the number of viewing zones N can be determined as

$$\mathrm{N} = \frac{\mathrm{W}}{e}. \tag{4}$$

As shown in Figure 3, these viewing zones appear to be in diamond shape in the top view. Each zone can be separated by eye base line into two triangles: the front triangle closer to the monitor and the rear triangle away from the monitor. Usually the viewing lateral range is as wide as the display plane, and the viewing zone R (for the right eye) and L (for the left eye) locate alternately from the display center. The most lateral viewing freedom is along the nominal viewing line, where it allows the greatest range of horizontal head movement and it is easiest to stay in the viewing zone. The most vertical (perpendicular to the display plane) viewing freedom is possible as long as the viewer stays within the viewing zone.

For the DTI monitor in our study, the number of viewing zones is determined as 7. A viewer can obtain stereo effect in 7 locations by adjusting their position laterally. It should be noted that these are the locations that perfect stereo effect is ensured. In fact, a viewer can move their head outside the range defined by the monitor width. Therefore, there are practically more than 7 zones where viewers can receive stereo effect. However, since the viewing direction is not right perpendicular to the monitor in this situation, the magnitude of the light transmitted to the viewer's eyes is significantly reduced. As a result, the stereo view becomes darker when the viewer positions are away from the screen center.

To facilitate the analytical study, a coordinate system is established as shown in Figure 3. Its origin is at the display center. The x and y (not shown in the figure) axes are parallel to the display frame. The z axis is perpendicular to the display pointing to the viewer, who is at a distance d from the display. Since we only consider the viewing zone in the horizontal plane passing through the display center,

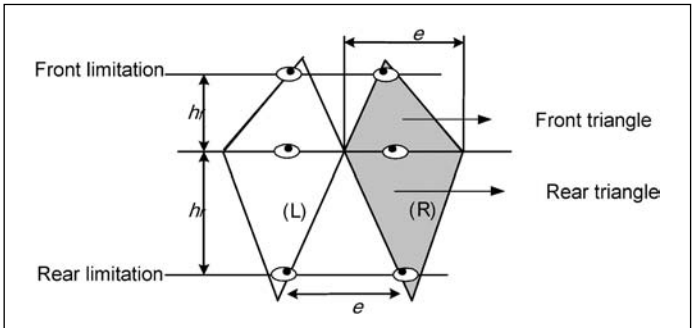

Figure 4. Viewing zone and viewing depth.

the y coordinate is constant 0 and only (x,z) coordinate pairs are given in the expressions.

For viewing zone n, starting from the center of the monitor and taking $\pm 1, \pm 2, \pm 3, \ldots$ for the right and left part of the screen, their (x,z) coordinates are (see Appendix for details)

For the front triangle $\Delta t_b t_c t_a$:

$$t_b: ((n-1)e,d); \qquad t_c: (ne,d); \qquad t_a: \left(\frac{(2n-1)\mathrm{W}e}{2(\mathrm{W}+e)}, \frac{\mathrm{W}d}{\mathrm{W}+e}\right). \tag{5}$$

For the rear triangle $\Delta t_b t_c t_d$:

$$t_b: ((n-1)e,d); \qquad t_c: (ne,d); \qquad t_d: \left(\frac{(2n-1)\mathrm{W}e}{2(\mathrm{W}-e)}, \frac{\mathrm{W}d}{\mathrm{W}-e}\right). \tag{6}$$

This study shows that the trapezoids of all viewing zones have the same area.

Of particular interest in the viewing zone geometry is the head movement perpendicular to the monitor plane, i.e., the viewing depth. Figure 4 is a detailed viewing zone and viewing depth illustration. The viewing depth that head can move without losing stereo effect is slightly different from the heights of the front and rear triangles. Denote the front and rear viewing depth off the nominal viewing line as h_f and h_r as shown in Figure 4, they can be determined as (see the Appendix for details):

$$h_f = \frac{ed}{\mathrm{W}+2e} \tag{7}$$

$$h_r = \frac{ed}{\mathrm{W}}. \tag{8}$$

According to Equations 7 and 8, the viewing depth is dependent on the monitor size, the viewing distance and eye base. It is also shown that the front viewing depth h_f is slightly smaller than the rear viewing depth h_r.

For our DTI monitor, the front and rear viewing depths are respectively calculated as 9.0 cm and 12.5 cm from the nominal viewing line, yielding a total of 22 cm continuous range for a viewer to adjust his or her position in the direction perpendicular to the screen plane.

Measurement Principles and AUTO3D Toolkit

Because of the unique principle of autostereoscope, its photogrammetric implementation requires some special considerations. First of all, the two images of a stereo pair should be interleaved in column to form the parallax stereogram. This is essentially a re-sampling process which is important to obtain correct and sharp stereo effect. Two options can be taken in this regard. As the first option, one may take odd columns from the left image and even columns from the right image to

form the parallax stereogram. This down-sampling process cannot use the full resolution of the original images and may not be allowed for high quality applications. The other option, which is chosen as default in our implementation, is to duplicate the rows of the two original images. This essentially double the image size for 3D display, however, as a trade-off the resolution of the original images is retained. Under this option, the full resolution of the original images is used.

The objective of photogrammetric measurement is to obtain the file or image coordinates of interest features. Because the displayed images are interleaved on the monitor, it is inconvenient to record and deduct screen coordinates of the interleaved 3D image. Instead, our measurements are recorded directly on the original left and right images. Each image is held by a display window which shows the current visible portion of the entire image. Each window has its own cursor and coordinate system. The two display windows are placed side by side in the monitor (see Figure 6). When the monitor is switched to 3D mode, the two images will be interleaved by columns to generate the parallax stereogram and provide the stereo effect. It should be noted this process not only displays the images in 3D mode, but all other contents in the windows such as cursors, symbols and drawings are also interleaved. This becomes another distinct consideration in autostereoscopic photogrammetric implementation and will be addressed below.

Because all graphics will be viewed in 3D mode during the autostereoscopic measurement process, they need to be designed identically and duplicated for each image window. In addition, the column-interleave property requires an unsymmetrical shape in 2D to achieve a symmetric appearance in 3D. Shown in Figure 5 are the designed point symbols in the left and right windows for 3D measurement. The two identical symbols should be used respectively for the left and right windows. Notice the symbol is not symmetric in terms of its horizontal dimension versus its vertical dimension. Two identical ellipses with major axes in vertical direction are used, and they will appear as one circular symbol when being viewed in the autostereoscopic mode. This design principle applies to any graphics or images that one would like to view as 2D feature under the autostereoscopic mode. As a consequence, this property may increase the amount of development for autostereoscopic photogrammetric applications.

Based on the above principles, a toolkit called AUTO3D was developed to conduct photogrammetric measurement with DTI monitor 2018XL. Its interface is made by Visual C++ 6.0 with Microsoft® Fundation Classes' Multiple Document Interface and Document/View framework. The toolkit can load, display and manipulate two images, conduct autostereoscopic measurement, label and export the results. Figure 6 shows the main image measurement windows. Notice there are four small 2D windows shown at the upper right corner of the main left and right image windows which are designed for monoscopic view. Users may need them under 3D mode to assure accurate 3D measurement. The four windows are a duplicate of two 2D image clips from the left and right images, respectively. The two identical left image clips and two identical right image clips are placed respectively apart at a distance of exactly half of the monitor width. In this way, they can be viewed without *x*-parallax under 3D mode.

A floating 3D cursor is specifically designed for the AUTO3D toolkit. The idea is to create two identical cursors and place them apart at exactly half of the monitor's width so that they can overlap under 3D mode. In 2D mode, the two cursors are one half as shown wide as in 3D mode and stay in the left and right windows, separately. Once the monitor is switched to 3D mode, the two cursors will be interleaved by column along with the images and any other graphics and be displayed as a floating cursor. In 3D measurement, the mouse movement will drive an equal and synchronized movement of the two cursors respectively in their own image windows. By rolling the mouse wheel, one can horizontally move the two images in the opposite direction to adjust the *x*-parallax. The combination of mouse movement and mouse wheel rolling can then accomplish the 3D measurement. To digitize points and get pixel information for further data analysis, the 3D cursor should be rested exactly on top of the feature. The viewer can evaluate this by checking the two pairs of small monoscopic windows

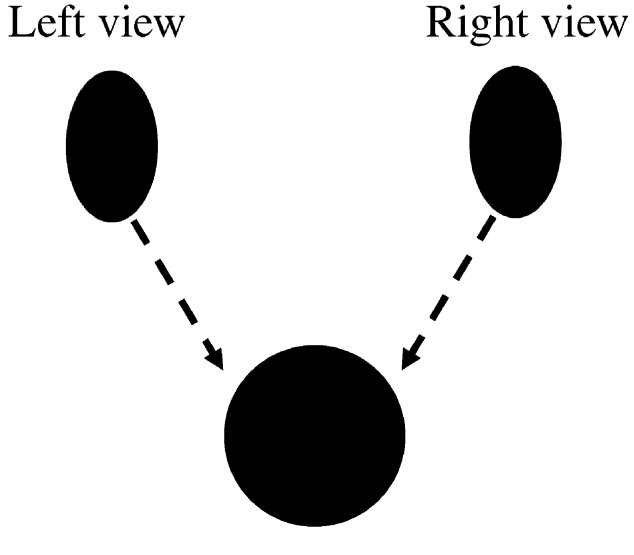

Figure 5. Dual and unsymmetrical graphic design.

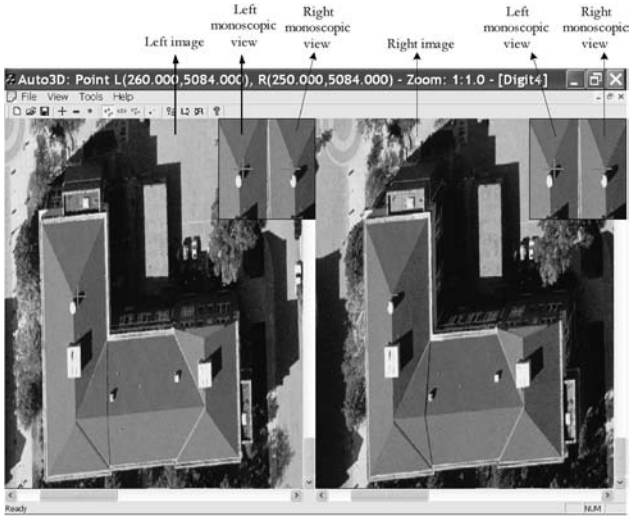

Figure 6. AUTO3D measurement interface (Purdue campus images, 2D mode).

under 3D mode (see Figure 6). This function has been proven very useful for inexperienced operators.

The AUTO3D toolkit has other functions to support photogrammetric measurement. As a preprocessing process, it provides two options to prepare the image files required by the 3D display. In the first option, one may duplicate the input image rows to double the vertical resolution. As an alternative, one may retain the odd columns of the left image and even columns of the right image to make the horizontal resolution half of the input images. To facilitate quality 3D view, the toolkit provides a set of image manipulation functions, including vertical image movement and rotation. They are useful for removing remaining *y*-parallax and making the photo base parallel to the eye base. Besides, users can display, locate, and edit the point symbols. The operator can label the feature points and record their pixel coordinates of the left and right images. Measurements can be color coded, stored into a file, and later loaded back to continue by adding new measurements or editing existing ones. These functions can ultimately be used to collect image features and determine their 3D ground positions.

Tests and Evaluation

Test Design

In order to evaluate the performance of autostereoscopic measurement, a stereo pair over Purdue University campus is used to conduct the tests. The original photo scale is about 1:4000 and scanned at a resolution of 30 μm. They are first epipolar normalized to remove *y*-parallax. The normalized images are then re-sampled to two resolutions, one at pixel size 25 μm and one at pixel size 50 μm, both of which will be used in our study.

Two types of well-defined feature points are selected for measurement. They consist of 18 points on the ground and 18 points on building roofs. Seven (7) geomatics engineering major graduate students without intensive stereoscopic or autostereoscopic training are involved in the tests. They are asked to measure all 36 feature points at two resolutions (25 μm and 50 μm) by following the specification prepared by the test organizer. In the specification, the exact location of each feature point is verbally described and illustrated with an image clip of 150 $\times$ 150 pixels. Figure 7 illustrates some of the selected feature points measured in the study.

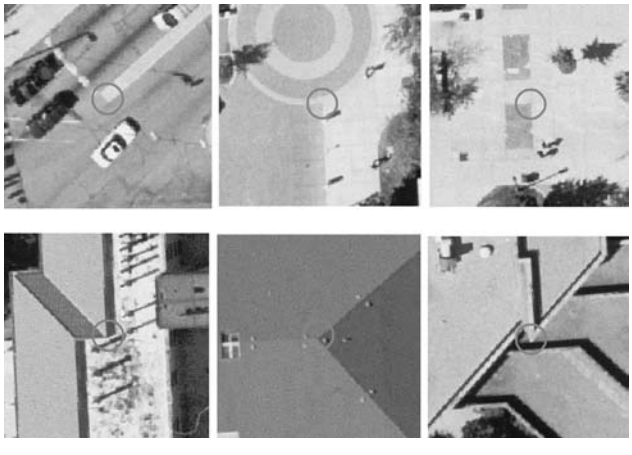

Figure 7. Examples of selected feature points for measurement (top row: ground; bottom row: roof).

For comparison purposes, the same images are also measured by the same group of operators using an ordinary digital photogrammetric workstation with Socet Set® package (developed by BAE Systems). A Dell UltraScan P991 19-inch Flat Trinitron CRT monitor with a resolution of 1024 $\times$ 728 pixels and NuVision 60GX stereo glasses (manufactured by MacNaughton, Inc.) are used for the stereoscopic measurement.

Results

Table 2 presents the statistics of the autostereoscopic and stereoscopic measurements. The values in the table are calculated in the following way. Let z_{ij} denote the coordinate measurement (x or y) at feature point i (i = 1,2, . . . n) by operator j (j = 1,2, . . . m). In our study, for each type of feature points (roof or ground), n = 18 and m = 7. The range, r_i, reflects the maximum difference among the 7 operators, namely, the difference between the maximum measured coordinate and minimum measured coordinate for the feature point i:

$$r_i = \max_j\{z_{ij}\} - \min_j\{z_{ij}\}. \tag{9}$$

The mean of such ranges at all points are calculated as follows:

$$\bar{r} = \frac{1}{n}\sum_{i=1}^{n} r_i. \tag{10}$$

The standard deviation (Std. Dev. in Table 2) is the variation of 7 operators at the measured feature points. They are calculated with the following equations:

$$\bar{z}_i = \frac{1}{m}\sum_{j=1}^{m} z_{ij}; \tag{11}$$

$$v_{ij} = z_{ij} - \bar{z}_i; \tag{12}$$

$$\sigma = \sqrt{\frac{1}{n}\frac{1}{m-1}\sum_{i=1}^{n}\sum_{j=1}^{m}(z_{ij} - \bar{z}_i)^2} \tag{13}$$

where Equation 11 is the average coordinate of all operators for point i, Equation 12 is the residual at point i, and Equation 13 is the standard deviation of all measurements. The above equations are applied to the roof points and ground points separately. The calculated mean range in Equation 10 and the standard deviation in Equation 13 are listed in Table 2. In addition, the table's last two columns list the arithmetic average of the statistics and the ratio between the averages obtained from the two resolutions. Such statistics are made respectively for the x coordinate measurements in the left and right images. Since the images are epipolar normalized, their y values are set as the same. Results in Table 2 are also shown in graphics within the following text to facilitate the comparison and analysis.

Consistency of Autostereoscopic Measurements

A few observations can be drawn from Table 2 and Figure 8 about the autostereoscopic measurement. First, the statistics from roof and ground measurements are close. Although there are certain inconsistencies in the measurements of the two feature types, no trend is observed and the variation tends to be random (see Figure 8), i.e., no one feature type can always get better measurement than the other. The maximum relative variation, occurring for the measurements at 25 μm resolution, is only 6 percent in the average statistics. This suggests that the autostereoscopic technology can accommodate large depth perception. It has no preference to certain feature type, and there is no significant identification and precision difference in measurement. The second observation drawn from Table 2 and Figure 8 is related to

TABLE 2. STATISTICS OF MEASUREMENTS (IN PIXELS, 25 μM/50 μM)

Method	Point Type	Statistics	*x*-Left	*x*-Right	*y*-Both	Average	Ratio
AUTO STEREO	Ground	Mean-range	3.50/2.43	3.90/2.10	4.22/2.46	3.87/2.33	1.7
		Std. Dev.	1.35/0.95	1.47/0.83	1.59/0.94	1.47/0.91	1.6
	Roof	Mean-range	4.34/2.14	3.01/2.43	4.40/2.88	3.92/2.48	1.6
		Std Dev.	1.55/0.86	1.16/0.88	1.66/1.14	1.47/0.97	1.5
STEREO	Ground	Mean-range	3.28/2.06	3.33/1.94	2.0/1.39	2.87/1.80	1.6
		Std. Dev.	1.26/0.93	1.28/0.79	0.88/0.59	1.14/0.77	1.5
	Roof	Mean-range	3.83/2.61	2.61/1.94	2.56/1.67	3.00/2.07	1.4
		Std Dev.	1.50/1.03	1.08/0.82	1.03/0.68	1.20/0.84	1.4

the consistency of measurements among different operators. Among the measurements of the 7 operators, the average range is 3.9 and 2.5 pixels, and the standard deviation is 1.5 and 0.9 pixels, respectively for the 25 μm and 50 μm resolution images. The range reflects the possible maximum errors in point identification and precision 3D perception among all the 7 participant operators. The standard deviation suggests that the statistical consistency among the participants is at the range of 0.9 to 1.5 pixels, which agree with the property of the on-screen measurement process that has a one-pixel expected measurement uncertainty. Third, the measurement precision decreases as the image resolution reduces, however, not at the same rate. Our results indicate that the precision decreases only by a factor of 1.6 (the last column of Table 2) while the resolution reduces from 25 μm to 50 μm by a factor of 2. This is a beneficial property when only limited resources are available to handle a large volume of data, because the photogrammetry accuracy loss is not as significant as the data resolution reduction. Finally, it is worthwhile noting that the maximum difference (range) of measurement errors is about 2.6 times the corresponding standard deviation. This fact is found to be true for all the scenarios in our tests: two types of features at two different resolutions. It essentially suggests that the measurement errors are consistent and follow the same or very similar distribution.

Comparison with Stereoscopic Measurements

The ordinary stereoscopic measurements with NuVision glasses and Socet Set® software are used as an independent reference to evaluate the autostereoscopic results. Their statistics are shown in Table 2 and Figure 9. Based on the comparison of Figure 8 and 9, and the results in Table 2, it can be concluded that the above four observations on perception depth, measurement consistency, measurement precision versus image resolution, and error distribution can also be made for the stereoscopic measurements. In other words, the autostereoscopic measurements present the same or very similar general properties as the stereoscopic ones.

The final analyses will be made on comparing the distribution and the overall statistics of the measurements. Presented in Figure 10 are the histograms for all of the measurement residuals calculated with Equation 12. In general, residuals from either technology and either resolution present a trend of Gaussian distribution, however, a detailed look reveals some differences. As is shown in Figure 10, for the 25 μm resolution the number of residuals within [−1,+1] pixels is 62 percent and 75 percent, respectively for the autostereoscopic and stereoscopic measurement. For the 50 μm resolution, the values are respectively 81 percent and 87 percent. This observation suggests that the stereoscopic measurements are more centralized than the autostereoscopic ones, and the higher the image resolution, the more decentralization occurs to the autostereoscopic measurements.

The summary statistics shown in Figure 11 support the above observation. It presents the overall difference of the two measurement technologies. For the 25 μm resolution, the standard deviation of all measurements is 1.5 and 1.2 pixels, respectively for the autostereoscopic and stereoscopic measurement. The values are respectively 0.94 and 0.81 pixels for the 50 μm resolution measurements. This suggests that the stereoscopic technology can yield more precise or better measurements than the autostereoscopic

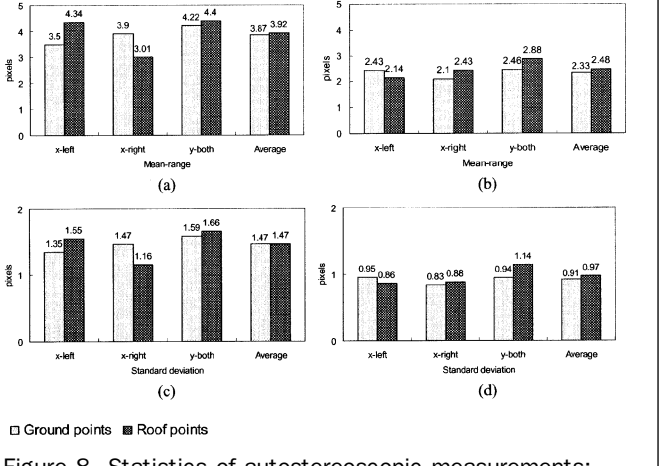

Figure 8. Statistics of autostereoscopic measurements: (a) 25 μm, (b) 50 μm, (c) 25 μm, and (d) 50 μm.

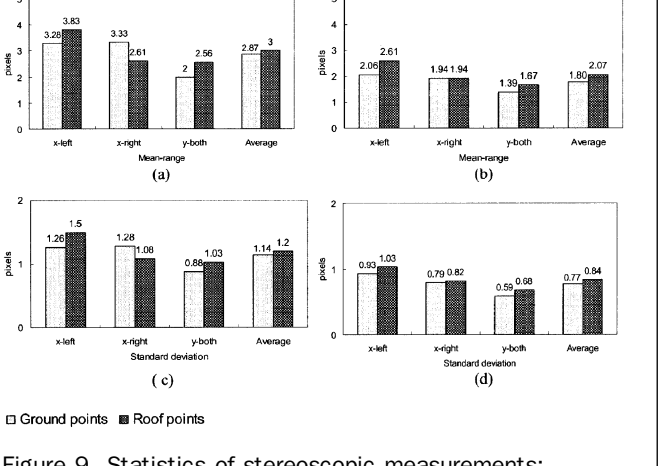

Figure 9. Statistics of stereoscopic measurements: (a) 25 μm, (b) 50 μm, (c) 25 μm, and (d) 50 μm.

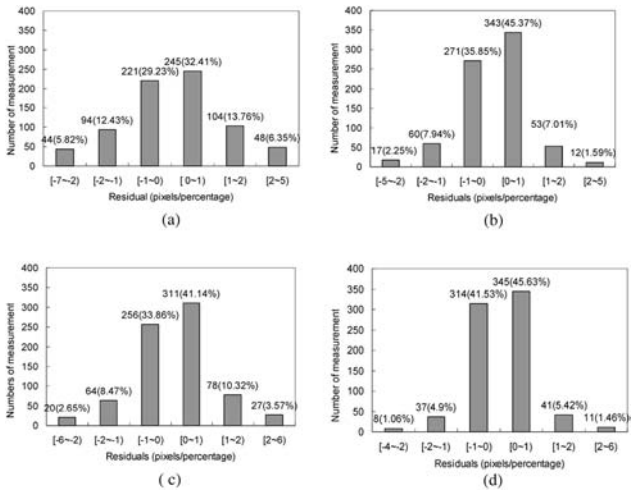

Figure 10. Distribution of total measurement residuals: (a) autostereo-25 μm, (b) autostereo-50 μm, (c) stereo-25 μm, and (d) stereo-50 μm.

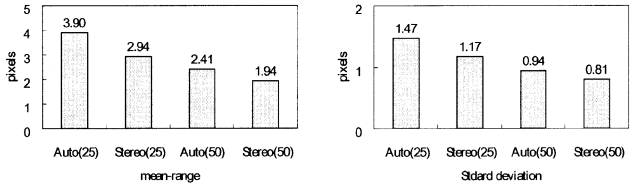

Figure 11. Overall statistics of autostereo and stereo measurements.

one. The higher the image resolution, the larger the precision difference between these two technologies. In our tests, the precision of autostereoscopic measurements are 25 percent (for 25 μm resolution) or 16 percent (for 50 μm resolution) lower than the stereoscopic ones.

This relatively lower precision is likely caused by the reduced brightness due to the use of LCD and illumination plate technologies in the DTI monitor. Since the light lines in the illumination plate can only occur every two pixels, the brightness of the DTI monitor should be lower than the conventional CRT monitor. To support this analysis, a light meter (Lux Meter LX1010B manufactured by Sinometer Instruments) is used to measure the brightness of the two monitors in a dark room, i.e., there is no other light source except the monitor. The monitors are tuned to their middle brightness and middle contrast, which are the same status when the image measurements are conducted. The light meter head contacts the monitor screen center. To reduce the effect of random measurement errors, three readings are obtained for each measurement and their average is listed in Table 3 for evaluation. In total, two measurements are obtained for each monitor. For the DTI monitor, the brightness measurements are respectively for its 2D and 3D modes; while the brightness of the CRT monitor is respectively obtained without and with the NuVision stereo glasses. As listed in Table 3, the 2D brightness of the DTI monitor is less than one-fourth (100/450) of the CRT monitor. The use of illumination plate for the DTI monitor and the stereo glasses

TABLE 3. BRIGHTNESS OF THE DTI AND CRT MONITORS

Monitor	Mode	Brightness (Lux)
DTI	2D	100
	3D	28
CRT	Without glasses (2D)	450
	With glasses (3D)	75

for the CRT monitor significantly reduces the brightness by a factor of 3.6 (100/28) and 6.0 (450/75). As a result, the DTI monitor is 2.7 (75/28) times less bright than the CRT monitor for 3D measurement.

Conclusions

Parallax barrier-based autostereoscopy is an affordable and implementable technology for goggle-free 3D image interpretation and photogrammetric measurement. Its stereoscopic effect and measurement capability become the key concerns for photogrammetric practice. This study develops the rigorous viewing zone geometry, and shows that the viewing effect is dependant on the design and specification of the 3D display. Viewers can obtain clear and correct stereo effect in a series of viewing zones of diamond shape. For the DTI monitor used in this study, analytical study shows this viewing zone can be as large as 22 cm in depth and minimum seven locations in lateral. Within this range, viewers have the freedom to adjust their positions while conducting autostereoscopic image interpretation and measurement.

Autostereoscopic measurement follows a principle similar to the common goggle-based measurement, however, with some fundamental distinctions. The two floating cursors must be fixed at a constant distance, whereas images need to be relatively moved to achieve 3D measurement. The images to be viewed in 3D mode should have a vertical resolution twice of the horizontal one to accommodate the column interleave requirement. All graphics, including cursors, symbols, user interface need to be designed in a dual and unsymmetrical manner, which eventually may complicate the development.

The autostereoscopic and stereoscopic technologies share common properties. Reduction in image resolution causes measurement precision decrease in an unequally proportional manner, which is a beneficial property when handling a large volume of data with limited resources. Measurement errors of both technologies follow the Gaussian distribution.

Our tests conclude that the autostereoscopic measurement is less precise than the stereoscopic one. Statistically, this means that the autostereoscopic measurements have larger range and larger variation, and are not as centralized as the stereoscopic ones. The higher the image resolution, the more different their measurement precision. For images at 25 μm resolution, it is shown that the autostereoscopic measurement precision is 1.5 pixels, 25 percent lower than the stereoscopic one. These are 0.9 pixels and 16 percent lower for images at 50 μm resolution. This precision difference is caused by the relatively lower brightness of the autostereoscopic monitor. Better results are expected with advancement in the autostereoscopic manufacture. Future work will be focused on enhancing current AUTO3D capabilities with feature extraction functions for field and mobile environments.

Acknowledgments

The work is sponsored by the National Geospatial-Intelligence Agency. Seven (7) graduate students participated in the measurement tests.

Appendix

This appendix derives the analytical expression of viewing geometry. Figure 3 shows the geometry of viewing zone for a planar autostereoscopic display. For simplicity, we consider the geometry in a horizontal plane passing the display center. The coordinate system orgin is at the display center, the x axis is parallel to the display plane, and the z axis is perpendicular to the display plane, pointing to the viewer. The viewer's left (L) and right (R) eyes are separated by the eye base e, and at a viewing distance d from the display plane. In Figure 3, s_1 is the screen right end, while s_2 is screen left end. W is the screen width. The front triangle right next to the center line is $\Delta t_b t_a t_c$ defined by the intersection of lines from s_1, s_2 and $z = d$.

Equation of line $\overline{s_1 t_b}$, passing through point $\left(\frac{W}{2},0\right)$ and $(0,d)$ is

$$z = \frac{-2d}{W}x + d. \tag{A-1}$$

Equation of line $\overline{s_2 t_c}$, passing through point $\left(-\frac{W}{2},0\right)$ and (e,d) is

$$z = \frac{2d}{W + 2e}x + \frac{Wd}{W + 2e}. \tag{A-2}$$

Solving Equation (A-1) and (A-2) yields the location of point t_a as $\left(\frac{We}{2(W + e)}, \frac{Wd}{W + e}\right)$. Similarly, the above derivation can be applied to the n^{th} triangle, whose front node's coordinates are $\left(\frac{(2n - 1)We}{2(W + e)}, \frac{Wd}{W + e}\right)$.

For the rear triangle, equation of line $\overline{s_2 t_b}$, passing through point $\left(-\frac{W}{2},0\right)$ and $(0,d)$ is

$$z = \frac{2d}{W}x + d. \tag{A-3}$$

Equation of line $\overline{s_1 t_c}$, passing through point $\left(-\frac{W}{2},0\right)$ and (e,d) is

$$z = \frac{-2d}{W - 2e}x + \frac{Wd}{W - 2e}. \tag{A-4}$$

From equation (A-3), (A-4) we can determine the coordinates of point t_d as $\left(\frac{We}{2(W - e)}, \frac{Wd}{W - e}\right)$. Applying the same derivation to the n^{th} triangle will yield its rear node coordinates as $\left(\frac{(2n - 1)We}{2(W - e)}, \frac{Wd}{W - e}\right)$.

For the front limitation h_f shown in Figure A-1, the similarity triangle geometry leads to

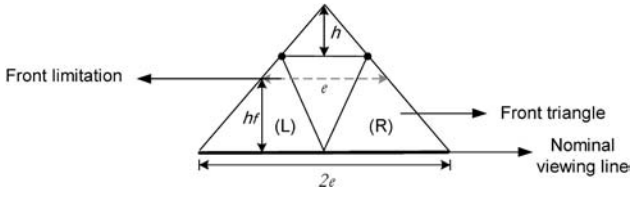

Figure A-1. Geometry of the front triangle and the limitation of viewer's movement.

$$\frac{h}{\frac{We}{W + e}} = \frac{h + \left(d - \frac{Wd}{W + e}\right)}{2e},$$

i.e., the front head movement range is

$$h_f = \frac{ed}{W + 2e}. \tag{A-5}$$

Similarly, we can obtain the relationship for the rear triangle:

$$\frac{h_r}{e} = \frac{\frac{Wd}{W - e} - d}{\frac{We}{W - e}}$$

This then yields the rear head movement range:

$$h_r = \frac{ed}{W}. \tag{A-6}$$

References

Bourke, P., 1999. Autostereoscopic lenticular images, URL: http://astronomy.swin.edu.au/~pbourke/stereographics/lenticular/index.html (last date accessed: 13 January 2006).

DTI Technologies, Inc., (2004). *User Manual for the DTI 2018XLQ/2018XLC Virtual Window*™.

Eichenlaub, J.B., and A.E. Martens, 1990. Stereo display without glasses, Advanced Imaging, Volume 5, Number 5:52–55.

Eichenlaub, J.B., 1993. The Parallax Illumination Autostereoscopic Method, *Stereo Computer Graphics and Other True 3D Technologies* (McAllister, D.F., editor), Princeton University Press, pp. 166–182.

Jones, E.R., and A.P. McLaurin, 1993. Three-Dimensional Imaging through Alternating Pairs, *Stereo Computer Graphics and Other True 3D Technologies* (McAllister, D.F., editor), Princeton University Press, pp. 214–229.

Kaplan, S.H., 1952. Theory of parallax barriers, *Journal of the Society of Motion Picture and Television Engineers*, Volume 59, pp. 11–21.

Okoshi, T., 1976. *Three Dimensional Imaging Techniques*, Academic Press New York.

Pastoor, S., and M. Wöpking, 1997. 3D Displays: A review of current technologies, *Displays*, Volume 17, pp. 100–110.

Petrie, G., 2001. 3D Stereo-viewing of digital imagery: Is autostereoscopy the future for 3D? *GeoInformatics*, Volume 4, Number 10:24–29.

Sexton, I., 1992. Parallax Barrier Display Systems, *IEEE Colloquium on Stereoscopic Television*, Volume Digest 173, pp. 5/1–5/5.

Son, J., V.V. Saveljev, Y. Choi, J. Bahn, S. Kim, and H. Choi, 2003. Parameters for designing autostereoscopic imaging systems based on lenticular, parallax barrier, and integral photography plates, *Optical Engineering*, 42(11):3326–3333.

Usery, E.L., 2003. Autostereoscopy – Three-dimensional visualization solution or myth? Proceedings of the Geospatial Visualization and Knowledge Discovery Workshop, 18–20 November, Lansdowne, Virginia, URL: http://www.ucgis.org/Visualization/whitepapers/usery-autostereoscopy.pdf (last date accessed: 13 January 2006).

(Received 17 July 2004; accepted 12 October 2004; revised 21 December 2004)